Chemical Science

Accepted Manuscript

Volume 9
Number 1
7 January 2018
Pages 1-268

Chemical Science

rsc.li/chemical-science

ISSN 2041-6539

ROYAL SOCIETY OF CHEMISTRY

EDGE ARTICLE
Xinjing Tang et al.
Caged circular siRNAs for photomodulation of gene expression in cells and mice

This is an Accepted Manuscript, which has been through the Royal Society of Chemistry peer review process and has been accepted for publication.

Accepted Manuscripts are published online shortly after acceptance, before technical editing, formatting and proof reading. Using this free service, authors can make their results available to the community, in citable form, before we publish the edited article. We will replace this Accepted Manuscript with the edited and formatted Advance Article as soon as it is available.

You can find more information about Accepted Manuscripts in the Information for Authors.

Please note that technical editing may introduce minor changes to the text and/or graphics, which may alter content. The journal's standard Terms & Conditions and the Ethical guidelines still apply. In no event shall the Royal Society of Chemistry be held responsible for any errors or omissions in this Accepted Manuscript or any consequences arising from the use of any information it contains.

ROYAL SOCIETY OF CHEMISTRY

rsc.li/chemical-science

ARTICLE

Tandem rigidification and π-extension as a key tool for the development of a narrow linewidth yellow hyperfluorescent OLED system.

Krzysztof Bartkowski,[‡, [a]]Paola Zimmermann Crocomo, [‡, [b]] Michał Andrzej Kochman, [‡, [c]]Dharmandra Kumar,[b]Adam Kubas,*[c] Przemysław Data,*[b] and Marcin Lindner*[a]

Hyperfluorescence (HF), a relatively new phenomenon utilizing the transfer of excitons between two luminophores, requires careful pairwise tuning of molecular energy levels and is proposed to be the crucial step towards the development of new, highly effective OLED systems. To date, barely few HF yellow emitters with desired narrowband emission but moderate external quantum efficiency (EQE <20%) have been reported. This is because a systematic strategy embracing both Förster Resonance Energy Transfer (FRET) and triplet to singlet (TTS) transition as complementary mechanisms for effective exciton transfer has not yet been proposed. Herein, we present a rational approach, which allows, through subtle structural modification, a pair of compounds built from the same donor and acceptor subunits, but with varied communication between these ambipolar fragments, to be obtained. The TADF-active dopant is based on a naphthalimide scaffold linked to the nitrogen of a carbazole moiety, which through introduction of an additional bond leads not only to π-cloud enlargement, but also rigidifies and inhibits rotation of the donor. This structural change prevents TADF, and guides bandgaps and excited state energies to simultaneously pursue FRET and TTS process. New OLED devices utilizing the presented emitters show excellent external quantum efficiency (up to 27%) and narrow full width at half maximum (40nm), which is a consequence of very good alignment of energy levels. The presented design principles prove that only a minor structural modification is needed to obtain commercially applicable dyes for HF OLED devices.

Introduction

Fundamental and applied studies of organic light-emitting diodes (OLEDs) have been encouraged by the rapid development of electronics such as smartphones, lighting, and flat panel displays.[1] The fluorescent (1st generation) and phosphorescent (2nd generation) OLED emitters,[2,3] which have been commercially available for 15 years, have suffered insufficient colour purity, poor efficiencies, and lifetimes, as well as high manufacturing costs. Subsequently, a 3rd generation of metal-free, thermally activated delayed fluorescent (TADF)[4–7] organic materials have been intensively explored within the last few years as promising candidates for commercial applications. The key feature of the operating mechanism of 3rd generation emitters is reverse intersystem crossing (rISC), in which the electron transfer proceeds from a triplet state to a singlet state. Light emission subsequently occurs by fluorescence from the singlet state. In most emitter compounds, the lowest singlet state is higher in energy than the lowest triplet state, meaning that rISC is a thermally activated process, and efficient rISC requires a small singlet-triplet energy gap (ΔE_{ST}). The minimization of ΔE_{ST} is therefore an important goal in the design and development of TADF materials.[8] A minimized ΔE_{ST} results in emission of the total population of available photons. A general strategy to achieve low ΔE_{ST} values is to enforce a spatial separation between the HOMO and the LUMO.[9,10] This design principle is implemented in donor-acceptor (D-A) molecular architectures where the electron-donating and electron-accepting moieties are partially decoupled from one another, for example, by a near-orthogonal orientation of the two moieties. Examples of this include cyanobenzene[11] and dicyanopyrazine-based moieties,[12] rigid heteroaromatic cores containing benzothiadiazole or oxazoles,[13,14] dibenzo- and multiring- phenazines,[15–21] heptazine,[22] and aromatic imides.[23–27] Despite tremendous progress made with this type of molecular engineering, a commonly encountered issue is a broad full-width at half-maximum (FWHM) ranging from 80 to 150 nm which is detrimental to colour purity.[28,29] Furthermore, triplet–triplet or singlet-triplet annihilation adversely impacts the roll-off efficiency as well as lowers operational lifetimes. A suitable approach to circumvent these problems could be the implementation of hyperfluorescence (HF) accelerated emission in OLED devices (4th generation of emitters).[30] This approach, pioneered by Adachi,[31] is based on the combination of a TADF
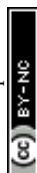
a. Institute of Organic Chemistry, Polish Academy of Sciences
Kasprzaka 44/52, 01-224 Warsaw (Poland)
b. Faculty of Chemistry, Silesian University of Technology, M. Strzody 9, 44-100, Gliwice (Poland)
c. Institute of Physical Chemistry, Polish Academy of Sciences
Kasprzaka 44/52, 01-224 Warsaw (Poland).
d. ‡ these authors contributed equally

ARTICLE

Journal Name

assistant dopant (A, see Figure 1) with a fluorescent emitter dopant (E, Figure 1) in a host matrix.

Because of the extraordinary electronic character (*vide supra*) the TADF-active molecule undergoes an effective excitation. Then, from the singlet state of the assistant dopant (S_1^A), excitons are transferred to the lower-energy singlet state of fluorescent dopant (S_1^E) . This transfer, called FRET (Förster Resonance Energy Transfer) plays a crucial role in the HF phenomenon. Excitons are pumped from the TADF dopant to the emissive species, which causes a spectacular increase in the emission efficiency. Benefits from FRET

states energies to concomitantly fulfil both requirements. Our hyperfluorescent dye system is based on a tandem rigidification-π-extension modification of a naphthalimide (**NI**) motif (shown in Fig. 1, right) containing a twisted D-A-(D) electronic structure (**2**, **4**) to an analogous, fully conjugated D-A architecture (**6**). Both flexible skeletons **2** and **4** exhibit TADF and high EQE when used as the emissive layer of OLED devices. Rigid but non-planar molecule **6** exhibits ordinary fluorescence with relatively poor EQE (up to 6%). A significant increase of emission efficiency is, however, noticed when compound **2** is doped with **6**, which can be assigned to both
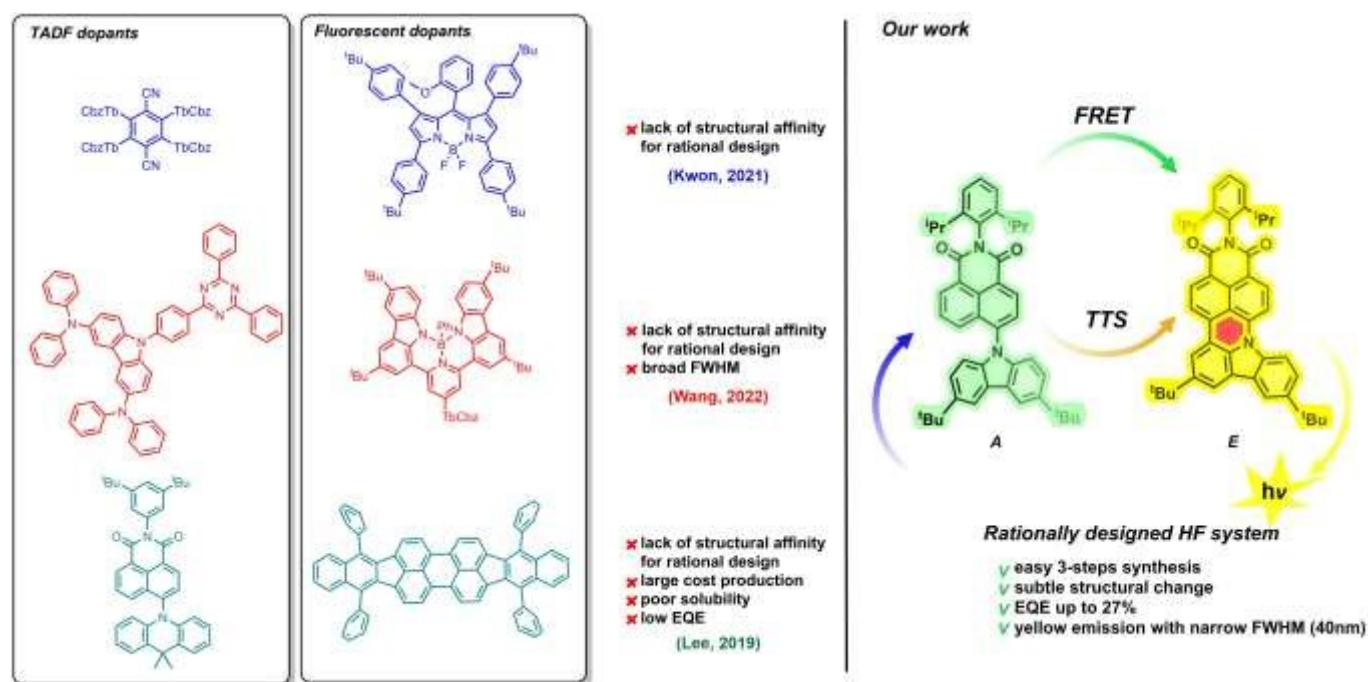

Figure 1. Current progress in the domain of green-to-yellow HF-OLED systems (left) and summary of the work presented herein (right).

include, not only higher quantum emission, but also the fine-tuning of the emission wavelength range. Both TADF and fluorescent dopants, however, must possess the proper optical properties. Experimentally this can be observed as a superposition of TADF-active and fluorescent emission and absorption wavelength ranges. Importantly, spectrally narrow emissions with efficient External Quantum Emissions (EQE) have been identified mostly for blue and green HF emitters[30–35], while pursuing both parameters at yellow and more bathochromically shifted regions is troublesome as most of the ongoing work in this space provides systems that do not exceed 20% EQE[34,36–41] or provide broad emission bands[42] (Figure 1). Therefore, prerequisite of emission/absorption overlap seems to be insufficient.

Along this line, Brédas and co-workers[43] showed theoretically that a double way of triplet harvesting is much more beneficial for HF process when S_1 energy of fluorescent dopant is only a slightly higher than T energy of TADF dopants. This allows, in parallel, RISC mediated singlet to triplet excitons transfer, followed by FRET and the direct triplet to singlet transfer (TTS) as to potentially yield 100% of internal quantum efficiency (IQE).

Facing this challenge, herein, we propose unprecedented molecular design leading to strict control under FMOs energy gap and excited

FRET and TTS phenomena. The EQE of the resultant hyperfluorescent OLED device is raised to 27% with a FWHM of 40nm. Effective energy transfer from TADF active **2** to the fluorescent dye **6** proves the efficacy of the proposed modification strategy.

Results and Discussion

To realize hyperfluorescent emitters *via* the proposed molecular strategy (*vide supra*), we designed **NI** based architectures with donor-acceptor-(donor) electronic structures, which are envisaged to act as TADF (I) and fluorescent (II) dopants. Their design principles embrace (I): utilization of a rigid scaffold with a limited number of rotating donors which could decrease ΔE_{ST} and HOMO-LUMO energy gaps, reducing the risk of nonradiative pathways from T_1, as well as to suppress unwanted Dexter energy transfer (DET); (II): increase conjugation and the rigidity of the entire π-system by fusing the **NI** core with an electron rich group (through formation of an addition six-membered ring, see Figure 1), which would result in the formation of a nonplanar, molecular arrangement which simultaneously switches off the TADF property. This structural deviation provides a handle to govern its excite state energies, absorption region, prevent undesired aggregation, and elevate the efficiency of the photoluminescence quantum yield

(PLQY). With these features in mind, the synthesis of the compounds **2**, **4** and **6** were performed within scalable 2-3 synthetic steps and are depicted in Scheme 1 (for the detailed procedures, see the ESI). The intermediates **1** and **3** were first synthesized *via* condensation between commercially available 4-bromo-1,8-naphthalic anhydride with 2,6-diisopropyl- or 4-bromo-2,6-dimethyl-aniline, respectively. Subsequently, Buchwald–Hartwig cross-coupling reactions with 3,6-ditertbutylcarbazole (TbCbz) gave emitters **2** and **4** in 71 and 59% yield. For **6**, an analogous synthetic pathway was employed to reach intermediate **5**, which was then subject to a one pot Buchwald–Hartwig cross-coupling/direct arylation reaction to provide the target molecule in an acceptable 40% yield.
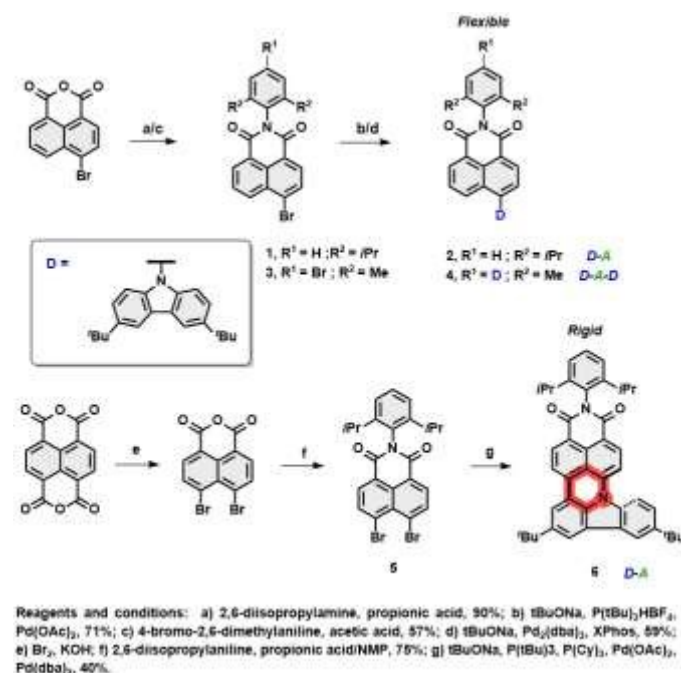
Scheme 1. The synthesis pathway towards emitters **2**, **4,** and **6.**

Crystallography

To evaluate the correlation between molecular arrangement of compounds **2**, **4,** and **6** and their optical features, X-ray quality single crystals were obtained by a slow evaporation from solutions of DCM, THF, and chloroform respectively. Compounds **2** and **4** crystallized in the monoclinic P2_1/*c* and orthorhombic P*bcn* space groups, with four molecules per unit cell. Deeper insight into their molecular structures, displayed in Figure 2, revealed a highly twisted conformation for both D-π-A, as well as the A-D-A triad, which is manifested by pronounced torsion angles (-113°, with respect to the plane determined by naphthalene bridge) between TbCbz and naphthalene backbone (exemplified for **2** in Figure 2A). This entails a minimization of the undesired intermolecular π-π interaction as the closest C-H···π distances (shown in Figure 2C/2E) were 5.15 Å (**2**) and 7.39 Å (**4**). Dye **6** crystallizes in the triclinic P-*1* space group with "head to tail" antiparallel alignment of two molecules in the primitive unit cell (Figure 2D). Intriguingly, a striking difference in its solid-state behavior can be noticed as the

twisting of TbCBz group is inhibited (see Figure 2B) through fusion with the NI core. The rationale for this modification was the rigidification of the entire skeleton and concurrent curvature introduced which is seen by the small torsion angles (-14.8°, 7.3°, Figure 2B).

Closer inspection of the packing mode of **6** (Figure 2D) unveils an extended 2D structure in the crystal lattice maintained *via* two, very weak, C-H···π interactions with distances between 3.47 Å and 3.63 Å (Figure 2D). This seems to be sufficient to avoid aggregation and guarantee spatial separation of FMOs as both structural parameters
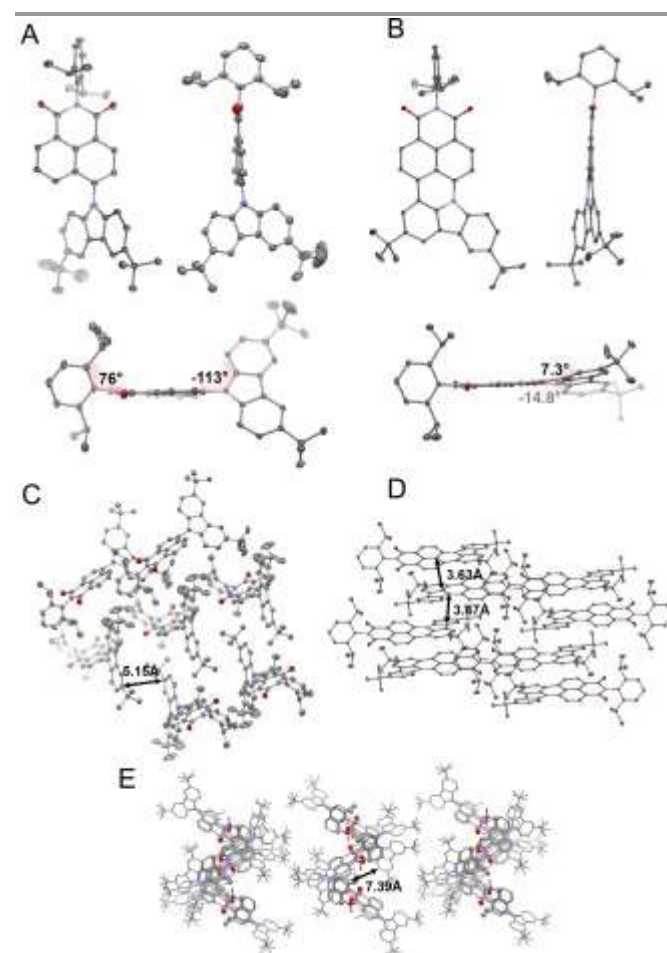

Figure 2. Crystallographic structures of **2** (A) and **6** (B). Space arrangement of **2** (C), **6** (D), and **4** (E). Thermal ellipsoids present 50% probability. Hydrogen atoms are omitted for the sake of clarity.

participate in the rational design of fluorescent structures.

Photophysics in solution and in the solid-state

Initially, we investigated the UV-vis absorption and emissive properties of **2**, **4**, and **6**. For the set of compounds, which differ from each other by the number of donors attached (**2** is a D-A, whereas **4** D-A-D type of emitter, respectively), UV-vis spectra (Figure 3) in both nonpolar and polar solvents shown transitions below 450 nm, similarly to other D-A derivatives of **NI**.[24] When it comes to compound **6**, a red-shift of the absorption maxima by 80 nm is observed with respect to **2** and **4** which hold twisted substituents. This is consistent with the increased conjugation of

ARTICLE

Journal Name

this molecule. Consecutively, the charge transfer characteristic and impact of polarity on the photoluminescence quantum yield were evaluated (Figure 3). For the set of D-A (**2**), D-A-D (**4**) type of emitters, we observed distinct positive solvatochromism

follow-up analysis in a solid matrix. Thus, two matrices were selected: the non-polar aliphatic medium Zeonex and a small molecule mCP (1,3-Bis(N-carbazolyl)benzene).
Based on the CV and HOMO-LUMO analysis (Figure S11, SI), mCP was chosen for OLED device application (Figure 4).
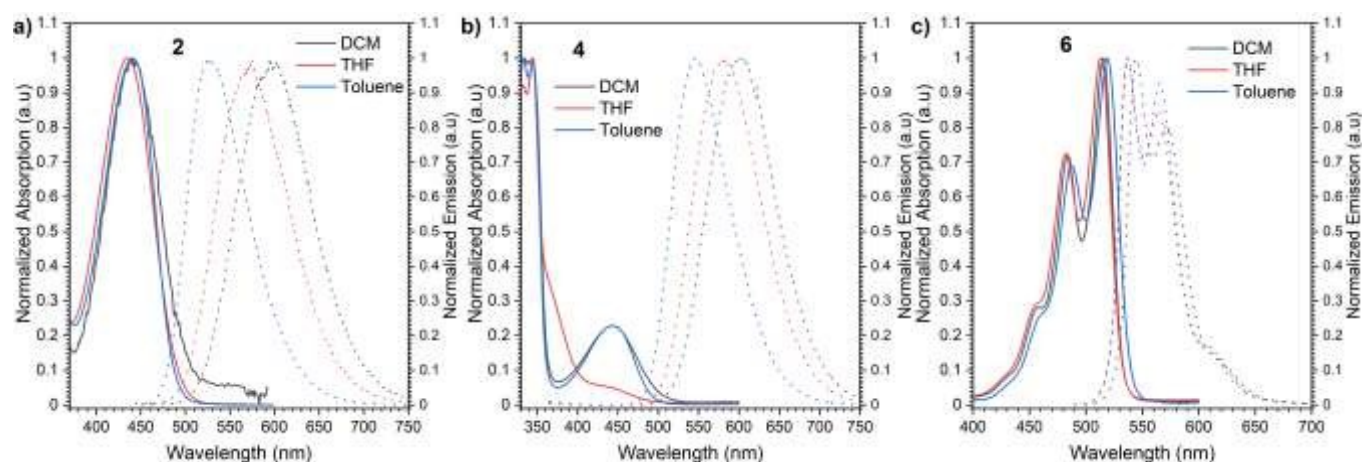

Figure 3. Normalized absorption and emission spectra of compound **2** (a), **4** (b), and **6** (c) in dichloromethane (DCM), tetrahydrofuran (THF) and toluene.

manifested by a strong, broad, emission band which shift to lower energies with increased solvent polarity. Such optical behaviour is typical for emission from the charge transfer state (^{1}CT). Accordingly, the PLQY also decreases with the increase of polarity (Table 1). Conversely, for compound **6**, in which the donor is fused with the acceptor and hence rotation around C-N bond is minimized, the solvent polarity only has a minimal impact. The emission has a vibronic structure which is a hallmark of a localized excited state (^{1}LE).

The most significant difference between these three emitters is that compounds **2** and **4** exhibit emission above microsecond delay time (Figure 4) while **6** only has a nanosecond emission profile (Figure 5). The lack of DF for **6** is clearly visible during oxygen quenching experiment. While spectrum of TADF active molecule **2** is rapidly changed upon exposure on oxygen, spectrum of **6** stays intact (see Figure S10, ESI). The rationale for this is the lack of motion between donor and acceptor moiety, which is related to rigidification (Thus, charge transfer is not observed (see Figure S11, SI), which is

Table 1. Summary of the general photophysical properties of compounds **2**, **4**, **6**.

Compound	λ_{em}, nm[a]	Host	PLQY %[b]	τ_{PF}, ns[c]	τ_{DF}, μs[d]	DF/PF[e]	E_a[f] eV	S_1 eV[g]	T_1, eV[g]	ΔE_{ST}, eV[h]
2	509	Zeonex	61	17.97	1.59	0.21	0.012	2.43	2.12	0.31
	536	mCP	87	14.21	20.43	2.49	0.075	2.31	2.08	0.24
4	518	Zeonex	4	14.97	1.478	0.75	0.028	2.40	2.09	0.31
	544	mCP	78	12.76	7.112	2.96	0.070	2.28	2.07	0.21
6	564	Zeonex	84	8.78	-	-	-	2.20	2.20	0.00
	567	mCP	95	9.21	-	-	-	2.19	2.19	0.00
1% **6** and 10% of **2**	567	mCP	97	53.50	8.81	8.79	0.029	2.19	2.09	0.10

[a] Photoluminescence maximum; [b] Photoluminescence quantum yield; [c] Prompt fluorescence lifetime in the host; [d] Delayed emission lifetime in the host; [e] Delayed fluorescence (DF) to prompt fluorescence (PF) ratio in the host; [f] Activation energy of the triplet to singlet transfer, [g] Singlet and triplet energy in host, based on emission maxima. Error ± 0.03 eV; [h] Singlet-triplet energy splitting in Zeonex. Error ± 0.05 eV.

Consequently, we switched further studies to the solid-state, due to the fact the main goal was to estimate the probability of using the

consistent with our previous observation in solution.

Journal Name ARTICLE

delay time. Nevertheless, closer inspection of the emission spectra around 300 K, above the microsecond delay time, suggests diverse emissive behaviour with respect to the host used. Dye **2** initially, above the 2.5 μ s, exhibits delayed emission similar to the prompt fluorescence, recognized as the TADF process. However, a tail, which intensity is enhanced significantly with further delay, is found as an RTP process. An analogous, but less pronounced effect was determined for compound **4** in the Zeonex matrix. Both emitters in

^{1}CT&^{1}LE. In this case and due to the higher ΔE_{ST} gap, there is a higher chance to observe the RTP process rather than TADF. As for the behaviour of the emitters in the mCP matrix, strong TADF emission was noticed which is even more favorable taking into consideration the high DF/PF parameter (close to 3) which suggests almost 100% of the triplet harvesting process (Table 1). On top of that, a very high PLQY in the mCP matrix, 87% for **2** and 78% for **4**, gives a promising perspective for TADF based OLED emitters. Using
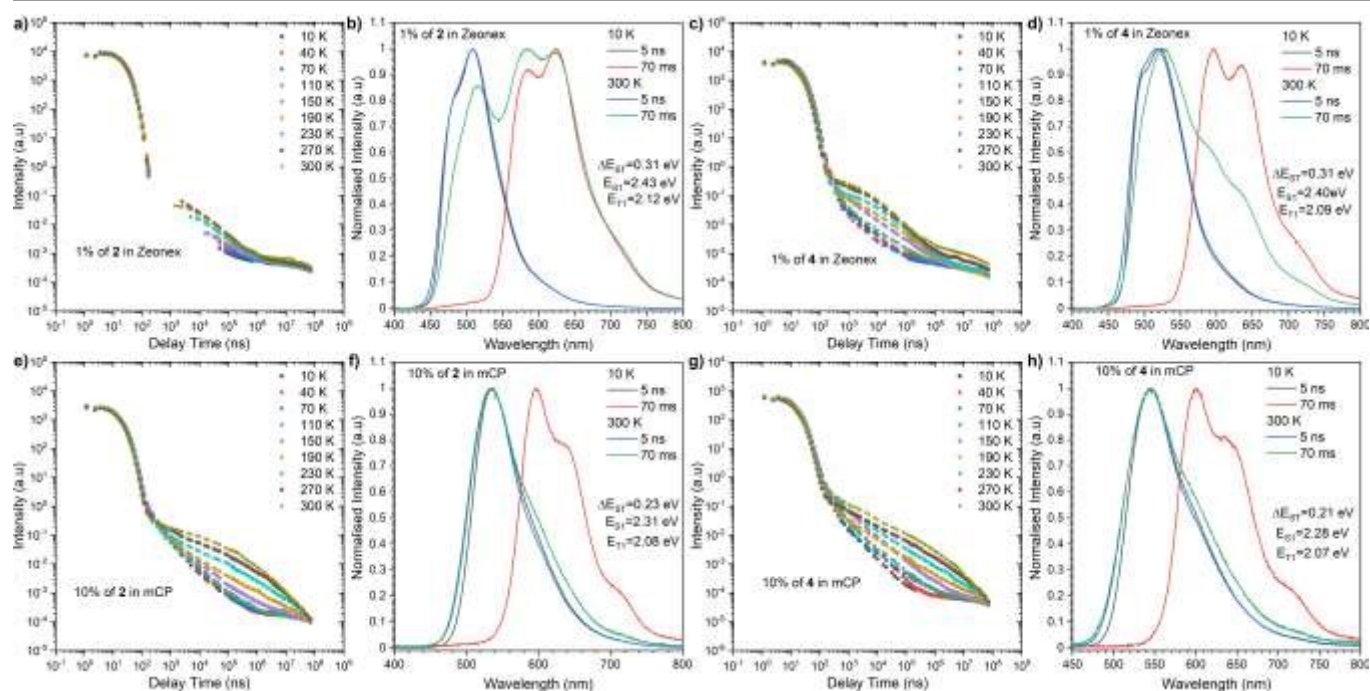
Figure 4. Time-resolved spectra and transient decays of thin films of compound **2** and **4** in Zeonex and mCP at different temperatures.

mCP matrix showed, however, different responses. Namely, the delayed emission coming through the TADF process starts to intensify above 300 ns (at 300 K) and is visible above 70 ms. A plausible explanation for this different behaviour needs a deeper insight into fluorescence emission showing a vibronic structure in the Zeonex matrix. This suggests the emission stemming from the ^{1}LE state (Figure 4b, d, Figure 5b) whereas in the mCP host the emission bears a ^{1}CT characteristic (Figure 4f, h). Among all emitters, the phosphorescence occurred from the localized excited state (^{3}LE). The dual delayed emission in Zeonex matrix, which appears rare, is not unprecedented in photophysical studies,[44,45] and could be elucidated based on the El-Sayed rule, in which the rate of (reverse) intersystem crossing is very high if the radiationless transition involves changing the type of the orbital. Transfer of the excited state between the ^{3}LE and ^{1}CT is such an example, but in the Zeonex matrix, the transfer is between ^{3}LE and ^{1}LE or mixed

equation 1, it is possible to estimate the theoretical maximum OLED external quantum efficiency (EQE), which in our case could be up to 26.1% for OLEDs based on compound **2** and 23.4% for compound **4**.

$$EQE = \eta_{out}\, \eta_{fl}\, \Upsilon\, \eta_{fr}$$ Eq. 1

where:

η_{out} is the outcoupling (usually it's 20-30% maximum outcoupling efficiency)

η_{fl} is the PLQY

Υ =1, the charge balance factor

η_{fr}= 1, which contributes to emission, for TADF emitter 100% singlet excitons are formed from charge recombination, 25% directly, 75% from triplet state rISC process.
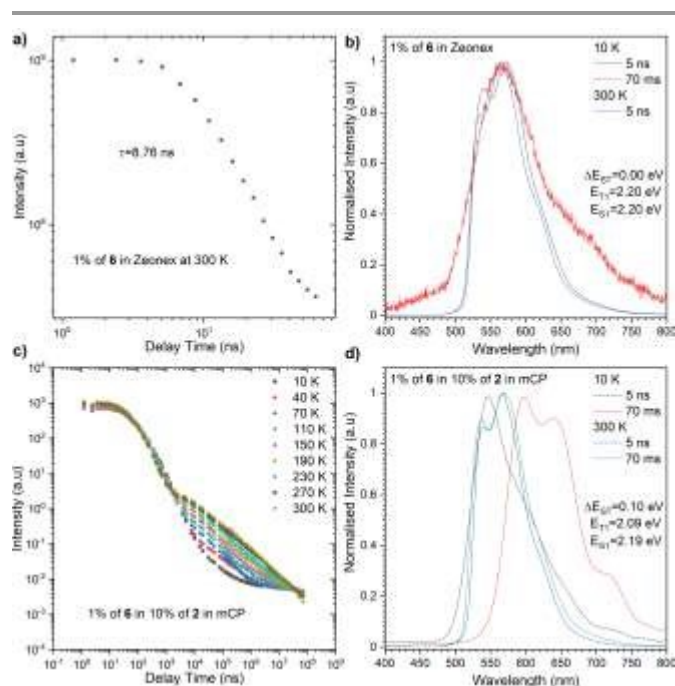
Figure 5. Photophysical characterisation of compound **6** in zeonex (a,b) and in 10% of 2 in mCP (c,d)
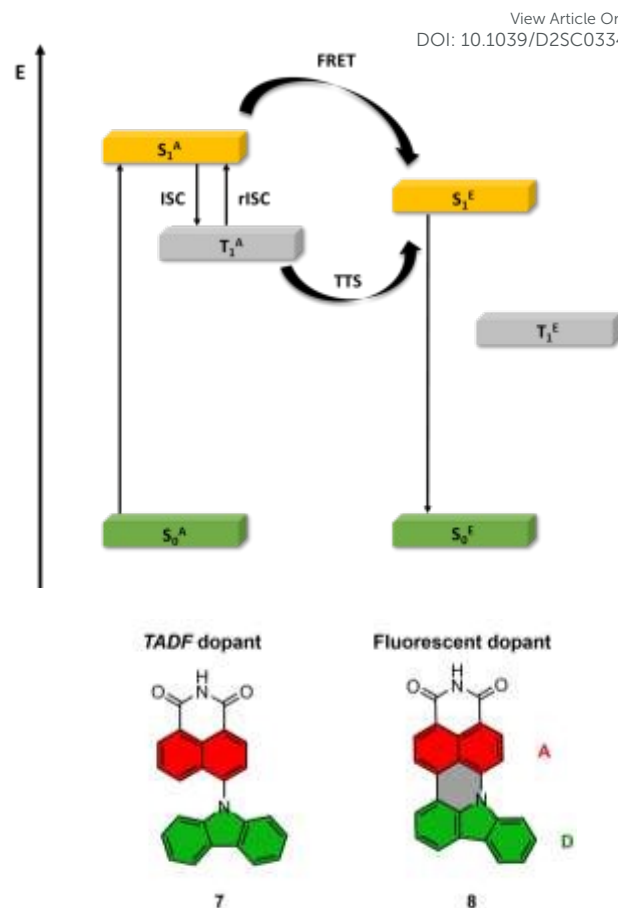

Figure 6. Energy diagram, for HF system, with the path towards double harvesting of triplet *via* FRET and TTS (above); molecular structures of truncated model compounds **7** and **8** (below).

The highest PLQY efficiency in mCP, was obtained for compound **6**, nevertheless, due to the fact that we only observed fluorescence emission in this compound, the parameter concerning the amount of excited state is η_{ff}= 0.25. This suggests the typical OLED structure will have an efficiency of up to 7% which is substantially smaller than for TADF based emitters. On the other hand, one can notice that because emitter **6** has no CT broad emission it is not affected by the matrix and the emission of compound **2** and partial emission of compound **4**, overlap the absorption spectra of compound **6** (Figure 3, 4, 5). The later factor paves the way towards the desired FRET process between TADF compound **2** and fluorescence emitter **6**. Fluorescence emission of the mixture of the compounds **2** and **6** in mCP has a similar structure to single emitter **6** in mCP and additional delayed emission was observed at 300K (Figure 5c,d).The later result is proof of the FRET process and is in addition to the obtained emissive hyperfluorescence structure. However, considering excited state energies for 2 and 6 given in table 1, FRET is not only a driving force of hyperfluorescence process. One can notice that a small energy difference between S-T state favours effective rISC transition, forcing subsequently a singlet-to-singlet transition. At the same time when the singlet energy of **6** lies solely 0.08 eV above the triplet energy of **2** (given in Table 1), TTS transition can occur according to the path shown in Figure 6 truly profiting of the overall population of available triplets.

Computational methods

To aid in the interpretation of the spectroscopic data for compounds **2**, **4** and **6**, we complemented their photophysics with electronic structure calculations. At the preliminary stage, we employed time-dependent density functional theory (TDDFT) in combination with the ωB97XD exchange-correlation functional.[46]

The results of these exploratory calculations are summarized in the Supporting Information.

For the sake of convenience, the compounds under study were represented by truncated model molecules in which the 2,6-dialkylphenyl ring was removed, and the dangling bond was saturated with a hydrogen atom. The two tert-butyl groups on the TbCbz moiety were likewise removed and replaced with hydrogen atoms. Thus, compounds **2** and **4** were jointly represented by model compound **7**, while compound **6** was represented by model compound **8** (see Figure 6 for truncated structures). Owing to the relatively smaller sizes of compounds **7** and **8**, we were able to treat their excited electronic states with a spin-opposite-scaled algebraic-diagrammatic construction method of second order (SOS-ADC(2)).[47–52]The SOS-ADC(2) method has previously been found to give accurate predictions for the energies of intra- and intermolecular charge transfer states of various organic donor-acceptor compounds and molecular clusters,[53–56] and we expect it to be reliable for the calculation of the optical properties of compounds **7** and **8.**

We begin the discussion of the simulation results by examining the vertical excitation spectra of model compounds **7** and **8**, which are given in Table 2. Accompanying this data, Figure S9 (SI) shows ground-state equilibrium geometries of both compounds, and EDDMs for their respective lowest singlet and triplet excited states.

Chemical Science

Journal Name ARTICLE

In compound **7**, where the D moiety is twisted with respect to the A moiety, the lowest singlet excited state (S₁) arises from

Table 2. Vertical excitation spectra of compounds **7** and **8** as calculated at the SOS-ADC(2)/cc-pVDZ level of theory: vertical excitation energies (ΔE) and associated oscillator strengths (f). μ is the (orbital-relaxed) electric dipole moment of the given state. The qualitative character of each excited state is given in brackets.

Compound	State	ΔE, eV	f	μ, D
7 (model of **2** and **4**)	S₀			2.4
	S₁ (D → A ICT)	3.767	0.132	15.7
	S₂ (A ππ*)	4.055	0.013	3.0
	S₃ (D ππ*)	4.156	0.064	1.5
	S₄ (A ππ*)	4.408	0.223	6.4
	T₁ (A ππ*)	2.890	0	3.1
	T₂ (D ππ*)	3.671	0	2.6
	T₃ (D → A ICT)	3.761	0	10.1
	T₄ (D ππ*)	3.914	0	2.1
8 (model of **6**)	S₀			5.3
	S₁ (D + A ππ*)	3.124	0.605	8.3
	S₂ (D + A ππ*)	3.755	0.004	6.5
	S₃ (D + A ππ*)	4.029	0.085	6.7
	S₄ (D + A ππ*)	4.218	0.001	7.3
	T₁ (A ππ*)	2.445	0	5.4
	T₂ (D + A ππ*)	3.332	0	6.5
	T₃ (D ππ*)	3.557	0	6.6
	T₄ (D + A ππ*)	3.860	0	5.7

intramolecular D → A charge transfer (ICT). Among the higher excited states, the S₂ and S₄ states are $\pi\pi$*-type states that are localized on the D moiety, while the S₃ state is a $\pi\pi$*-type state localized within the A moiety. The S₁ state has a higher oscillator strength (0.132) than either the S₂ or the S₃ states, which indicates that the first photoabsorption band of compound **7** arises predominantly from the S₀ → S₁ transition. This conclusion can be safely extrapolated to compounds **2** and **4**.
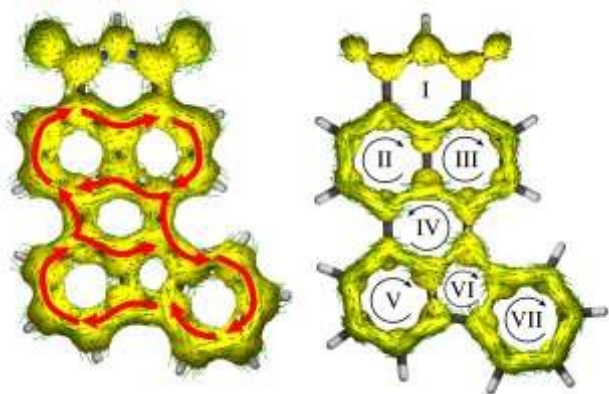

Figure 7. ACID of **8** (left) and the π-bonding system of **8** (right), plotted in the form of isosurface with an isovalue of 0.05 a.u. The direction of the diatropic ring current within the whole molecule is indicated with red arrows. Curly arrows show direction of ring currents within each ring. The magnetic field vector is perpendicular to the plane of the heavy atom skeleton and points towards the viewer.

The lowest triplet state of compound **7** (T₁) is localized on the A moiety. It is essentially a counterpart of the T₁ ($^3B_{2u}$) state of unsubstituted naphthalene, which is dominated by a HOMO→LUMO excitation.[69]

Moving to compound **8**, the additional linkage between the electron-donating and -accepting moieties has a strong effect on the electronic structures of the low-lying singlet states. In compound **8**, the S₁ state is a $\pi\pi$*-type state that is delocalized over both the D and the A moieties, and it does not show a substantial ICT character. States S₂ to S₄ are likewise nonpolar. The S₁ state has a high oscillator strength, and it is well separated in energy from the higher singlet excited states. It follows that the first photoabsorption band of compound **8** arises mainly from the intense S₀ → S₁ transition. By extrapolation, the same applies to compound **6**.

The T₁ state, on the other hand, remains largely localized on the A moiety, and it is similar to the T₁ ($^3B_{2u}$) state of naphthalene.

To gain more insight into the photoluminescence properties of the systems under study, we optimized minima on the potential energy surfaces (PESs) of the S₁ and T₁ states of compounds **7** and **8**. Figure 6 shows the general idea of the HF systems energy levels with marked FRET and rISC of TADF dopant, while Figure S6 presents the detailed results of the described analysis. We found that the selected model compounds meet the necessary conditions for acting as a FRET energy donor and acceptor pair. Namely, the calculated vertical S₁ → S₀ fluorescence emission energy of compound **7**, at 3.159 eV, coincides closely with the calculated vertical S₀ → S₁ absorption energy of compound **8**, which is 3.124 eV. This observation indicates that FRET can indeed occur from the photoexcited compound **7** onto compound **8**. Furthermore, the minimum on the S₁ state of compound **8** is located considerably lower in energy (more specifically, by 0.876 eV) than the vertical energy of the S₁ state of compound **7** at its ground-state equilibrium geometry. This means that FRET from compound **7** onto compound **8** is effectively a one-way process; the electronic excitation cannot be transferred back onto compound **7**.

Extrapolating to compounds **2**, **4**, and **6**, we expect that unidirectional FRET likewise takes place from photoexcited compounds **2** and **4** onto compound **6**.

Lastly, Figure 7 shows the ACID plots of molecule **8**. To elucidate how strong the communication between donor and acceptor moieties is we distinguished global ring current (with contribution of both, σ and π MOs; Figure 8, left) and π MOs part (Figure 8, right). Such a representation allowed us to present the competition between global and local delocalization within model molecule **8**. Both, TbCbz and naphthalene subunits are involved in the global diatropic current pathway as well as each staying as individual aromatic systems. Thus, even the local diatropic ring currents along the **NI** and TbCbz are present, the global aromaticity is a dominant phenomenon, in accordance to the observed spectroscopic properties. For only π MOs ACID plot communication is significantly weaker. The donor (rings V, VI and VII) is only weakly coupled to the acceptor moiety (rings I, II, and III). Inspection of the directions of the ring currents indicates that within both naphthalene and TbCbz moieties a diatropic current is present, while the flow path of current along ring IV, which is located in between the donor and the acceptor subunits is slightly paratropic.

ARTICLE

Nevertheless, skeleton **8** is fully conjugated, even though the communication involves σ and π MOs. Analysis of experimentally observed ^{1}H NMR spectra of **2** and **6** (see SI) showed down-field shifted signals of the TbCbz moiety (up to 1 ppm) confirming the enhancement of diatropic current within whole conjugated skeleton including the donor subunit. This observation, aided by the computational analysis of skeletons **7** and **8**, *per analogiam,* to structures **2** and **6** confirms that the presented strategy of π-delocalization extension and rigidification can be a useful tool for designing of HF active compounds.
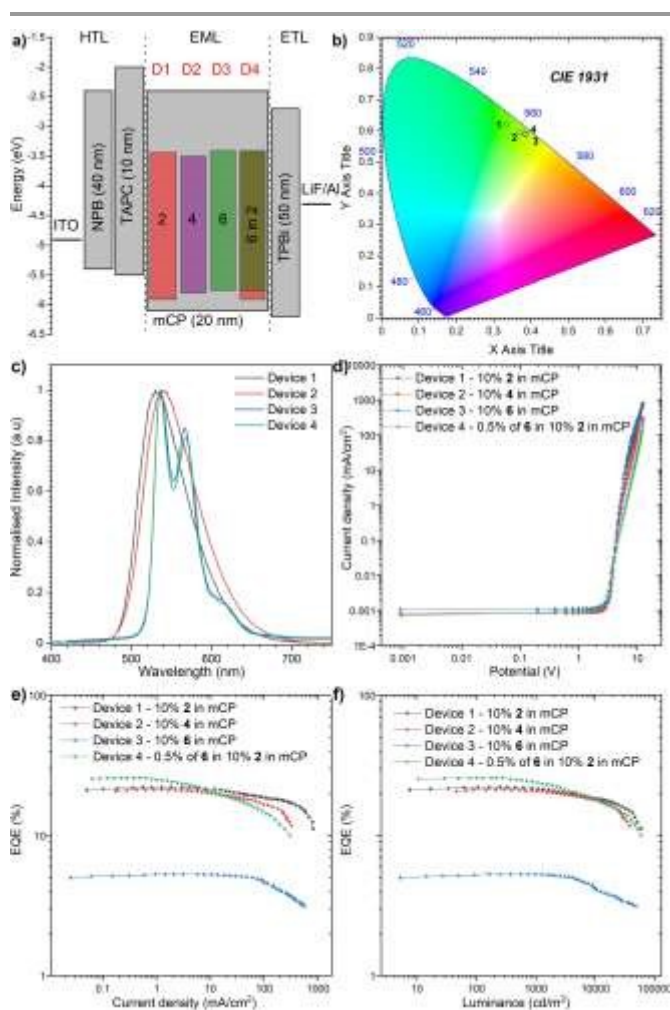
Figure 8. The characteristics of the OLED devices: a) device configuration; b) CIE diagram of emission colours; c)Electroluminescence spectra; d) Current density-bias characteristics; e) EQE-current density characteristics; f) Luminance-current density characteristics.

OLED devices

To investigate the applicability of the synthesized emitters, OLED devices were fabricated and characterized. The compounds were purified by sublimation before use. The investigated compounds were used as dopants in a mCP matrix which was suitable based on the obtained HOMO, LUMO, singlet and triplet energies. The OLED structures were deposited using high-vacuum thermal evaporators. Devices 1－3: ITO/NPB (40 nm)/TAPC (10 nm)/10% **2, 4,** and **6** in mCP (20 nm)/TPBi (50 nm)/LiF (1 nm)/Al (100 nm), Device 4:

ITO/NPB (40 nm)/TAPC (10 nm)/0.5% **6**, 10% **2** in mCP (20 nm)/TPBi (50 nm)/LiF (1 nm)/Al (100 nm) as was illustrated at Figure 8a.

The electroluminescence spectra of the measured devices correspond to the green-yellow region and match well with the photoluminescence spectra obtained from the initial photophysical analysis (Figure 8b). The electrical turn-on voltage is low and similar for all devices at around 2.7 V. In terms of the "classical" efficiency, the highest was for device 1 based on compound **2**, up to 22.1%. Devices 2 and 3 had up to 21.1% and 5.3% respectively (Figure 8c). These values are a slightly lower than the maximum theoretical values discussed above, nevertheless, the outcoupling factor varies between 20-30%, which suggests in our case we had 100% of the IQE (Internal Quantum Efficiency). An intriguing result was obtained for the hyperfluorescence structure, where the OLED EQE was 27% (Figure 8e) exceeding all "classical" TADF devices.

The highest luminance was measured for Device 1 with compound **2** with a value close to 59 000 cd/m^2 (Figure 8d). Nevertheless, the luminance behaviour was also very promising, in all the devices, the value exceeds 30 000 cd/m^2, which together with high efficiency qualifies it for commercial OLED applications. Furthermore, comparision with recently reported yellow HF-OLED devices (Figure 9) places the presented emitter system as one of the most promising to date.

Conclusions

In conclusion, a new rational strategy for hyperfluorescent dye systems was proposed. Rigidification of a TADF active dopant with simultaneous extension of π electron conjugation by introduction of only one new C-C bond allowed us to obtain a pair of two highly effective emitters.

Photophysical properties of the investigated compounds were consistent with our presumption and both TADF active molecules showed a similar optical response. Thus, separation of an additional TbCbz donor group by a benzene ring suppresses the communication between it and the acceptor. Because of this, the dopant **2** was chosen as the first component for the hyperfluorescent system.

Computational analysis of the designed molecules revealed that for both dyes **2** and **4**, the effective intramolecular charge transfer from donor to acceptor moieties is dominating, while for molecule **6** the main contribution of ππ* transition is observed. Further, ACID plots analysis was performed and the effective global conjugation within
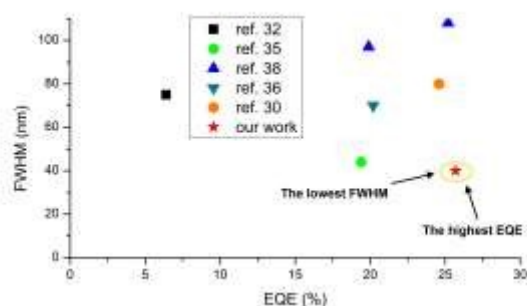

Figure 9. Summarized results of to-data reported yellow HF-OLEDs. For refs. 30, 32 and 36 FWHM values were estimated based on reported EL spectra.

View Article Online

the whole skeleton of **6** was confirmed, followed by ^{1}H NMR spectra analysis that was consistent with theoretical calculations. Thus, rationally designed rigidification of a twisted donor-acceptor scaffold can be used as a way of obtaining a globally delocalized skeleton with a bathochromically shifted absorption/emission maximum. This can indeed afford fine-tuning of excites states energies to realize simultaneously realized FRET and TTS transitions.

OLED devices utilizing dyes **2**, **4,** and **6** were prepared and characterized. Acceptable EQE for OLEDs based on **2** and **4** were recorded due their TADF activity. Fluorescent dopant **6** showed classical behaviour as the emissive layer. A hyperfluorescent device obtained by doping the emissive layer with **2** and **6**, however, showed excellent EQE (27%) and FWHM (40 nm), in accordance with that expected for a HF OLED system. Additionally, this represents the first, to the best of our knowledge, yellow HF OLED device, which exhibits such impressive performance.

The presented findings shed light on the potential of our proposed strategy for the design of the new fluorescent dopant structures which is relevant for the future successful development of 4th generation of OLED materials. Slight structural modification, allowing rigidification with simultaneous enhancement of π delocalization of the whole skeleton has led us to establish a simple method for the creation of efficient HF system of emitters.

Author Contribution

M.L. conceived and supervised the project; K.B and M.L. designed, synthesized, and characterized all emitters; P.Z.C and K.D carried out basic photophysical and time-resolved spectroscopic studies, fabricated and analysed OLED devices, while P.D. analysed and interpreted spectroscopic results; M.A.K and A.K. performed the computational studies; ML conceptualized the manuscript. K.B., M.A.K. A.K, P.D and M.L. contributed to writing the manuscript

Conflicts of interest

There are no conflicts to declare.

Acknowledgements

Notes and references

‡The data that support the findings of this study are available in the Supporting Information of this article. The calculated equilibrium geometries of the compounds under study were deposited at https://repod.icm.edu.pl/dataset.xhtml?persistentId=doi:10.18150/NZ5GFF

1   N. Thejo Kalyani and S. J. Dhoble, *Renewable and Sustainable Energy Reviews*, 2015, **44**, 319–347.
2   *Organic Light-Emitting Devices*, Springer New York, New York, NY, 2004.
3   *Highly Efficient OLEDs with Phosphorescent Materials*, Verlag GmbH & Co. KGaA, Weinheim, 2007.
4   H. Uoyama, K. Goushi, K. Shizu, H. Nomura and C. Adachi, *Nature*, 2012, **492**, 234–238.
5   M. Y. Wong and E. Zysman-Colman, *Advanced Materials*, 2017, **29**, 1605444.
6   J. M. Ha, S. H. Hur, A. Pathak, J.-E. Jeong and H. Y. Woo, *NPG Asia Materials*, 2021, **13**, 53.
7   Y.-Z. Shi, H. Wu, K. Wang, J. Yu, X.-M. Ou and X.-H. Zhang, *Chemical Science*, 2022, **13**, 3625–3651.
8   P. Data and Y. Takeda, *Chemistry – An Asian Journal*, 2019, **14**, 1613–1636.
9   P. de Silva, *The Journal of Physical Chemistry Letters*, 2019, **10**, 5674–5679.
10   J. Ehrmaier, E. J. Rabe, S. R. Pristash, K. L. Corp, C. W. Schlenker, A. L. Sobolewski and W. Domcke, *The Journal of Physical Chemistry A*, 2019, **123**, 8099–8108.
11   I. S. Park, S. Y. Lee, C. Adachi and T. Yasuda, *Advanced Functional Materials*, 2016, **26**, 1813–1821.
12   D. Karthik, Y. H. Jung, H. Lee, S. Hwang, B. Seo, J. Kim, C. W. Han and J. H. Kwon, *Advanced Materials*, 2021, **33**, 2007724.

ARTICLE

Journal Name

Chemical Science Accepted Manuscript

13   Y.-K. Wang, C.-C. Huang, S. Kumar, S.-H. Li, Z.-L. Dong, M.-K. Fung, Z.-Q. Jiang and L.-S. Liao, *Journal of Materials Chemistry C*, 2018, **6**, 10030–10035.

14   F. Ni, Z. Wu, Z. Zhu, T. Chen, K. Wu, C. Zhong, K. An, D. Wei, D. Ma and C. Yang, *Journal of Materials Chemistry C*, 2017, **5**, 1363–1368.

15   P. Data, P. Pander, M. Okazaki, Y. Takeda, S. Minakata and A. P. Monkman, *Angewandte Chemie International Edition*, 2016, **55**, 5739–5744.

16   J.-X. Chen, K. Wang, C.-J. Zheng, M. Zhang, Y.-Z. Shi, S.-L. Tao, H. Lin, W. Liu, W.-W. Tao, X.-M. Ou and X.-H. Zhang, *Advanced Science*, 2018, **5**, 1800436.

17   J. Chen, Y. Xiao, K. Wang, D. Sun, X. Fan, X. Zhang, M. Zhang, Y. Shi, J. Yu, F. Geng, C. Lee and X. Zhang, *Angewandte Chemie International Edition*, 2021, **60**, 2478–2484.

18   U. Balijapalli, Y. Lee, B. S. B. Karunathilaka, G. Tumen-Ulzii, M. Auffray, Y. Tsuchiya, H. Nakanotani and C. Adachi, *Angewandte Chemie International Edition*, 2021, **60**, 19364–19373.

19   Z. Cai, X. Wu, H. Liu, J. Guo, D. Yang, D. Ma, Z. Zhao and B. Z. Tang, *Angewandte Chemie*, 2021, **133**, 23827–23832.

20   J. Chen, W. Tao, W. Chen, Y. Xiao, K. Wang, C. Cao, J. Yu, S. Li, F. Geng, C. Adachi, C. Lee and X. Zhang, *Angewandte Chemie International Edition*, 2019, **58**, 14660–14665.

21   U. Balijapalli, R. Nagata, N. Yamada, H. Nakanotani, M. Tanaka, A. D'Aléo, V. Placide, M. Mamada, Y. Tsuchiya and C. Adachi, *Angewandte Chemie International Edition*, 2021, **60**, 8477–8482.

22   J. Li, T. Nakagawa, J. MacDonald, Q. Zhang, H. Nomura, H. Miyazaki and C. Adachi, *Advanced Materials*, 2013, **25**, 3319–3323.

23   M. Li, Y. Liu, R. Duan, X. Wei, Y. Yi, Y. Wang and C.-F. Chen, *Angewandte Chemie International Edition*, 2017, **56**, 8818–8822.

24   W. Zeng, H.-Y. Lai, W.-K. Lee, M. Jiao, Y.-J. Shiu, C. Zhong, S. Gong, T. Zhou, G. Xie, M. Sarma, K.-T. Wong, C.-C. Wu and C. Yang, *Advanced Materials*, 2018, **30**, 1704961.

25   T. Chen, C. Lu, Z. Chen, X. Gong, C. Wu and C. Yang, *Chemistry – A European Journal*, 2021, **27**, 3151–3158.

26   Z. Huang, Z. Bin, R. Su, F. Yang, J. Lan and J. You, *Angewandte Chemie International Edition*, 2020, **59**, 9992–9996.

27   X. Zeng, Y.-H. Huang, S. Gong, P. Li, W.-K. Lee, X. Xiao, Y. Zhang, C. Zhong, C.-C. Wu and C. Yang, *Materials Horizons*, 2021, **8**, 2286–2292.

28   Z. Yang, Z. Mao, Z. Xie, Y. Zhang, S. Liu, J. Zhao, J. Xu, Z. Chi and M. P. Aldred, *Chemical Society Reviews*, 2017, **46**, 915–1016.

29   G. Hong, X. Gan, C. Leonhardt, Z. Zhang, J. Seibert, J. M. Busch and S. Bräse, *Advanced Materials*, 2021, **33**, 2005630.

30   K. Goushi, K. Yoshida, K. Sato and C. Adachi, *Nature Photonics*, 2012, **6**, 253–258.

31   a) H. Nakanotani, T. Higuchi, T. Furukawa, K. Masui, K. Morimoto, M. Numata, H. Tanaka, Y. Sagara, T. Yasuda and C. Adachi, *Nature Communications*, 2014, **5**, 4016; b) P. Data, A. Kurowska, S. Pluczyk, P. Zassowski, P. Pander, R. Jedrysiak, M. Czwartosz, L. Otulakowski, J. Suwinski, M. Lapkowski, A.P. Monkman *Journal of Physical Chemistry C* **2016**, *120*, 2070–2078

32   D. Zhang, X. Song, A. J. Gillett, B. H. Drummond, S. T. E. Jones, G. Li, H. He, M. Cai, D. Credgington and L. Duan, *Advanced Materials*, 2020, **32**, 1908355.

33   D. Zhang, L. Duan, C. Li, Y. Li, H. Li, D. Zhang and Y. Qiu, *Advanced Materials*, 2014, **26**, 5050–5055.

34   D. Zhang, X. Song, M. Cai, H. Kaji and L. Duan, *Advanced Materials*, 2018, **30**, 1705406.

35   D. Zhang and L. Duan, *Nature Photonics*, 2021, **15**, 173–174.

36   J. H. Kim, K. H. Lee and J. Y. Lee, *Chemistry – A European Journal*, 2019, **25**, 9060–9070.

37   A. Shahalizad, A. Malinge, L. Hu, G. Laflamme, L. Haeberlé, D. M. Myers, J. Mao, W. G. Skene and S. Kéna-Cohen, *Advanced Functional Materials*, 2021, **31**, 2007119.

38   D. Zhang, X. Song, M. Cai and L. Duan, *Advanced Materials*, 2018, **30**, 1705250.

39   Y. H. Jung, D. Karthik, H. Lee, J. H. Maeng, K. J. Yang, S. Hwang and J. H. Kwon, *ACS Applied Materials & Interfaces*, 2021, **13**, 17882–17891.

40   J. H. Kim, K. H. Lee and J. Y. Lee, *Journal of Materials Chemistry C*, 2020, **8**, 5265–5272.

41   Z. Li, X. Hu, G. Liu, L. Tian, H. Gao, X. Dong, T. Gao, M. Cao, C.-S. Lee, P. Wang and Y. Wang, *The Journal of Physical Chemistry C*, 2021, **125**, 1980–1989.

42   G. Meng, L. Liu, Z. He, D. Hall, X. Wang, T. Peng, X. Yin, P. Chen, D. Beljonne, Y. Olivier, E. Zysman-Colman, N. Wang and S. Wang, *Chemical Science*, 2022, **13**, 1665–1674.

43   E. Cho, M. Hong, Y. S. Yang, Y. J. Cho, V. Coropceanu and J.-L. Brédas, *Journal of Materials Chemistry C*, 2022, **10**, 4629–4636.

44   R. Huang, J. Avó, T. Northey, E. Chaning-Pearce, P. L. dos Santos, J. S. Ward, P. Data, M. K. Etherington, M. A. Fox, T. J. Penfold, M. N. Berberan-Santos, J. C. Lima, M. R. Bryce and F. B. Dias, *Journal of Materials Chemistry C*, 2017, **5**, 6269–6280.

45   T. Hofbeck, U. Monkowius and H. Yersin, *J Am Chem Soc*, 2015, **137**, 399–404.

46   J.-D. Chai and M. Head-Gordon, *Physical Chemistry Chemical Physics*, 2008, **10**, 6615.

47   A. B. Trofimov and J. Schirmer, *Journal of Physics B: Atomic, Molecular and Optical Physics*, 1995, **28**, 2299–2324.

48   A. Köhn and C. Hättig, *The Journal of Chemical Physics*, 2003, **119**, 5021–5036.

49   S. Grimme, *The Journal of Chemical Physics*, 2003, **118**, 9095–9102.

50   Y. Jung, R. C. Lochan, A. D. Dutoi and M. Head-Gordon, *The Journal of Chemical Physics*, 2004, **121**, 9793–9802.

51   S. Grimme, L. Goerigk and R. F. Fink, *Wiley Interdisciplinary Reviews: Computational Molecular Science*, 2012, **2**, 886–906.

52   N. O. C. Winter and C. Hättig, *The Journal of Chemical Physics*, 2011, **134**, 184101.

53   A. A. J. Aquino, I. Borges, R. Nieman, A. Köhn and H. Lischka, *Physical Chemistry Chemical Physics*, 2014, **16**, 20586–20597.

54   M. A. Kochman and B. Durbeej, *The Journal of Physical Chemistry A*, 2020, **124**, 2193–2206.

55   F. Siddique, M. Barbatti, Z. Cui, H. Lischka and A. J. A. Aquino, *The Journal of Physical Chemistry A*, 2020, **124**, 3347–3357.

56   A. Tajti, B. Kozma and P. G. Szalay, *Journal of Chemical Theory and Computation*, 2021, **17**, 439–449.

Chemical Science Accepted Manuscript